Journal of Materials Chemistry B

ROYAL SOCIETY OF CHEMISTRY

PAPER

View Article Online
View Journal | View Issue

Cite this: J. Mater. Chem. B, 2024, 12, 7626

Simultaneous photoactivation of a fluoroquinolone antibiotic and nitric oxide with fluorescence reporting†

Tassia J. Martins,‡[a] Cristina Parisi,‡[a] Juliana Guerra Pinto,[b] Isabelle de Paula Ribeiro Brambilla,[b] Barbara Melilli,[c] Danilo Aleo,[c] Juliana Ferreira-Strixino[b] and Salvatore Sortino *[a]

The achievement of smart pharmaceuticals whose bioactivity can be spatiotemporally controlled by light stimuli is known as photopharmacology, an emerging area aimed at improving the therapeutic outcome and minimizing side effects. This is especially attractive for antibiotics, for which the inevitable development of multidrug resistance and the dwindling of new clinically approved drugs represent the main drawbacks. Here, we show that nitrosation of the fluoroquinolone norfloxacin (**NF**), a broad-spectrum antibiotic, leads to the nitrosated bioconjugate **NF–NO**, which is inactive at the typical minimum inhibitory concentration of **NF**. Irradiation of **NF–NO** with visible blue light triggers the simultaneous release of **NF** and nitric oxide (NO). The photouncaging process is accompanied by the revival of the typical fluorescence emission of **NF**, quenched in **NF–NO**, which acts as an optical reporter. This permits the real-time monitoring of the photouncaging process, even within bacteria cells where antibacterial activity is switched on exclusively upon light irradiation. The mechanism of photorelease seems to occur through a two-step hopping electron transfer mediated by the lowest triplet state of **NF–NO** and the phosphate buffer ions or aminoacids such as tyrosine. Considering the well-known role of NO as an "unconventional" antibacterial, the **NF–NO** conjugate may represent a potential bimodal antibacterial weapon activatable on demand with high spatio-temporal control.

Received 13th June 2024,
Accepted 8th July 2024

DOI: 10.1039/d4tb01291g

rsc.li/materials-b

Introduction

Multidrug resistance (MDR) in bacteria is the prime example of bacterial adaptation and the pinnacle of evolution and remains one of the major public health threats of the 21st century.[1–3] This concern and the dwindling of new clinically approved antibacterial drugs (only two new classes of antibiotics have been introduced into the clinic over the last two decades), represent the main obstacles to successfully treating bacterial diseases.[4] Another critical issue that makes the above scenario even worse is the occurrence of severe adverse off-target effects.[5] They arise especially for long-term antibacterial treatments and eventually can lead to autoimmune disorders, obesity and allergy.[6–8] Therefore, developing novel therapeutic approaches to fight MDR and reduce the exposure to antibiotic drugs in the body is desperately needed and represents one of the most challenging goals in human health care.[9] In this regard, the emerging field of photopharmacology holds high potential to improve the therapeutic outcome while minimizing the off-target side effects.[10–13] Antibiotic photopharmacology is based on the temporary inactivation of conventional antibiotics by their covalent linking with a photoresponsive moiety. This component can be designed to operate either irreversibly or reversibly. In the former case it is a photocleavable group, namely a photocage, which liberates the antibiotic under its active form upon light excitation. In the latter case it is a photoisomerizable component, namely an optical photoswitch, which remains always linked to the antibiotic, permitting the activity of the whole molecular construct to be reversibly switched on and off using light sources of different wavelengths.[10–13] In both cases, using light as a remote activation mechanism permits the biological activity of the antibiotic to be spatio-temporally controlled with high precision. Light is a non-invasive stimulus, easy to manipulate and ensures the confinement of the site of action of the photoactivatable drug at the illuminated area by the appropriate positioning of the

[a] PhotoChemLab, Department of Drug and Health Sciences, University of Catania, I-95125, Italy. E-mail: ssortino@unict.it
[b] Laboratory of Photobiology Applied to Health, Research and Development Institute, University of Vale do Paraíba, Urbanova I-2911, Brazil
[c] MEDIVIS S.r.l., Tremestieri Etneo, 95030 Catania, Italy

† Electronic supplementary information (ESI) available: Synthetic and experimental procedures. See DOI: https://doi.org/10.1039/d4tb01291g

‡ Equally contributed.

light beam and the accurate control of the therapeutic doses by tuning the light intensity and the irradiation time.[14] Compared with the better-known antibacterial photodynamic therapy (PDT),[15] based on the generation of the highly cytotoxic singlet oxygen,[16] that has already found applications in clinics,[17] the above-mentioned photopharmacological approaches are not dependent on the presence of oxygen, representing a significant advantage to also treating anaerobic bacteria, where PDT fails.

Fluoroquinolones (FQs) are a successful class of broad-spectrum, synthetic antibiotics.[18,19] Although widely used for treating general bacterial infections, FQs have seen a significant rise in antibiotic-resistant bacterial strains.[20] Besides, several safety concerns regarding their therapeutic use are still being raised by the FDA.[21] FQs have also been demonstrated to induce undesired photosensitivity side effects, including phototoxicity and photocarcinogenesis, upon undesired and uncontrolled environmental light absorption.[22–25] These processes are primarily associated with photodefluorination reactions,[26–29] a very uncommon event in the arena of fluoroaromatics due to the strength of the C–F bond (dissociation energy *ca.* 523 kJ mol^{-1}).[30]

Photopharmacological approaches have successfully faced the above limitations by controlling the antibacterial activity of FQs, exploiting both photoswitches and photocages activatable by biocompatible visible light.[31–40]

In the frame of novel antibacterial modalities, nitric oxide (NO) represents a promising alternative to conventional antibiotic drugs. Besides playing a multifaceted role in the bioregulation of vital functions in living bodies,[41,42] this inorganic free radical has been demonstrated to be an excellent antibacterial with a broad spectrum of action.[43–45] Interestingly, NO exhibits important advantages over conventional antibiotics, such as (i) absence of MDR,[46] (ii) multi-target reactivity,[47] (iii) confinement of its cytotoxic action over distance <200 μm, as a result of its half-life of *ca.* 1 s.[41]

Due to its transient nature, the antibacterial effects of NO are strictly dependent on its generation site and, analogously to other therapeutics, also from its doses.[48] This dependence has made the NO precursors activatable by light stimuli, usually named NO photodonors (NOPDs), appealing given the high spatiotemporal control light-triggering offers.[49–52]

Based on these considerations, in this contribution, we devised a smart bioconjugate in which a FQ antibacterial is temporarily inactivated by integrating a nitroso group within its molecular skeleton. This work aims to exploit the FQ chromophore as a photocage capable of generating NO and simultaneously restoring the FQ in its active form upon light excitation. Besides being motivated by the critical need to achieve novel photopharmaceuticals, the present work has been further encouraged by merging our ongoing interest in developing NOPDs[49,53,54] and our past interest in studying the photoreactivity of FQs.[29,55–59] As a proof of concept, we focused herein on norfloxacin (**NF**), a FQ used in the treatment of several bacterial diseases, including urinary tract infections in humans,[60] enteritis in dogs,[61] and chronic respiratory disease in chickens.[62]

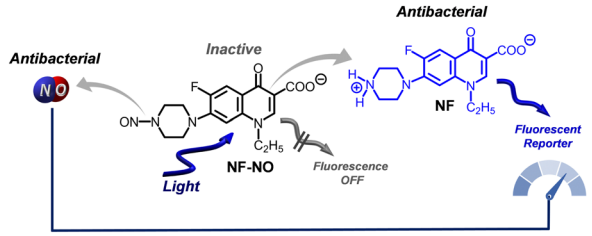

Scheme 1 Molecular structure of the most abundant prototropic species of **NF–NO** and **NF** present at physiological pH of 7.4. Irradiation of the inactive and low fluorescent **NF–NO** leads to the simultaneous generation of NO and the highly fluorescent **NF**.

This choice is not random but based on the following: (i) the nitroso-derivative (**NF–NO**) formed by biotransformation has been reported to have minimum inhibitory concentrations (MICs) higher than that of **NF** for several different bacteria,[63] (ii) the photochemical behaviour of **NF** has been well elucidated.[58,64,65]

Here, we show that the nitroso-derivative **NF–NO**, in which both **NF** and NO are reciprocally caged, is inactive towards ATCC *S. aureus* under dark conditions at a concentration in which NF is active (Scheme 1). Irradiation of **NF–NO** with visible blue light completely suppresses the photodefluorination, the main photodegradation pathway of **NF** and common to many FQs, and, in contrast, triggers the release of NO liberating **NF** in its active form. It is also shown that the characteristic fluorescence emission of **NF** is quenched in the **NF–NO** and restored after the release event (Scheme 1). This makes **NF** a proper optical reporter, permitting to follow its release and that of the equivalent amount of NO, in real-time, even within bacteria cells. Insights into the photorelease mechanisms are also reported.

Results and discussion

Spectroscopic properties and photolysis

NF–NO was easily obtained by nitrosation of **NF** in one step (see ESI†). Fig. 1 shows the spectroscopic features of **NF–NO** and, for the sake of comparison, those of **NF** in phosphate buffer at neutral pH. Like other structurally related FQs,[65] due to the ionization of the carboxylic group and the 4′-amino of the piperazinyl ring, **NF** may exist in three different prototropic forms in aqueous solution depending on pH and possessing distinct absorption and emission properties.[57] Given that the isoionic pH is *ca.* 7.4,[28] the zwitterionic form dominates at physiological pH (see Scheme 1). Nitrosation of the piperazinyl ring makes the related nitrogen less basic and thus, it is non-protonated at physiological pH. Therefore, **NF–NO** presents as an anion under these experimental conditions (Scheme 1).

The absorption spectra shown in Fig. 1A show that despite the spectral profiles of **NF–NO** changes only slightly if compared to **NF**, it exhibits a new absorption band in the UV region at 230 nm and, although not very intense, an extension of its absorption in the visible region well beyond 400 nm (see inset

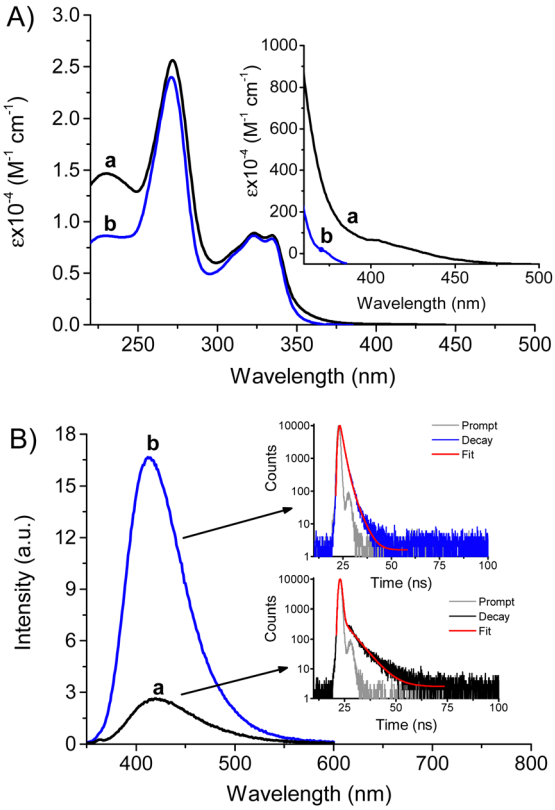

Fig. 1 (A) Absorption spectra of **NF–NO** (a) and **NF** (b) in PBS solution (10 mM, pH 7.4). The inset shows a magnified view of the absorption region beyond 360 nm. (B) Fluorescence emission spectra (λ_{exc} = 324 nm) of **NF–NO** (a) and **NF** (b) in PBS solution (10 mM, pH 7.4), T = 25 °C. The insets show the fluorescence decay (λ_{exc} = 370 nm; λ_{em} = 415 nm) and the related bi-exponential fitting.

Fig. 1A). This latter feature permits **NF–NO** excitation with visible blue light (*vide infra*).

Similar to other FQs,[65] **NF** shows an intense blue emission at physiological pH characterized by fluorescence quantum yield Φ_F = 0.11 and a bi-exponential decay with a dominant component (*ca.* 90%) having a lifetime τ = 1.5 ns (spectrum **b** and related inset in Fig. 1B). This emission is significantly quenched in **NF–NO** (Φ_F = 0.015) showing a red-shift of the emission maximum of *ca.* 15 nm and a shortening of the lifetime to τ = 0.5 ns (spectrum a and related inset in Fig. 1B). **NF–NO** remains stable for at least one month in the dark under these experimental conditions, as proven by the unaltered absorption and emission spectra.

As anticipated, the absorption of **NF–NO** extending in the visible region beyond 400 nm permits excitation of this compound with blue light. Fig. 2A reports the absorption spectral changes observed upon blue light irradiation of an air-equilibrated solution of **NF–NO**. They show the bleaching of all the main absorption bands, which is more evident in the band at 230 nm. Besides, the band at 275 nm slightly shifted to the blue. This spectral evolution is in line with the formation of **NF** as a stable photoproduct, which is characterized by a less intense absorption of the 230 nm band and absorption maximum of the 275 nm band blue-shifted if compared to **NF–NO** (see spectra a and b in Fig. 1A). Accordingly, the evolution of the fluorescence emission spectra upon irradiation shows a significant revival of the blue emission accompanied by a blue-shift of the emission maximum from 425 nm to 411 nm, all features typical of the **NF** fluorophore (Fig. 2B). The high fluorescence contrast in the samples before and after irradiation is also visible even at the naked eye (see images in Fig. 2B).

UHPLC-MS analysis was then carried out with the authentical **NF–NO** and **NF** samples. The chromatograms reported in Fig. 2C unambiguously confirmed this latter as the main stable photoproduct.

NF photouncaging implies, of course, the photogeneration of stoichiometric amounts of NO. Direct and indirect methods demonstrated photogeneration of this radical species through an ultrasensitive NO electrode and the typical diaminonaphthalene (DAN) assay (see ESI†), respectively. Amperometric monitoring allows NO to be directly detected with nM concentration sensitivity. As shown in Fig. 3A, **NF–NO** is stable in the dark but releases NO upon blue light excitation. According to an exclusively photoregulated process, NO generation stops as the light is turned off and restarts again as the illumination is switched on. Besides, the DAN assay, one of the most sensitive and selective fluorescence-based methods for indirect NO detection as nitrite (the main oxidation product of NO), showed the formation of fluorescence emission and excitation spectra typical for the fluorescent probe after its reaction with nitrite, only in the case of the irradiated samples (Fig. 3B).

An important aspect to be highlighted is that the high fluorescence contrast ratio between **NF** and **NF–NO** (see Fig. 2B) makes the former a suitable optical self-reporter,[53] giving readable and real-time information about the amount of **NF** and NO photogenerated. The quantum yield for the uncaging process, Φ_u, was estimated to be *ca.* 0.1. Although affected by a quite large error due to the low absorbance value at the excitation wavelength, the order of magnitude of Φ_u is worthy of note. In fact, despite the low absorption of **NF–NO** in the blue region, the high efficiency of the photouncaging process permits the release of sufficient amounts of **NF** and NO (μM range) within moderate time irradiation. Note that the absorption and emission photolysis profiles reported in Fig. 2 were very similar in the N_2-saturated solution (data not shown), suggesting that the efficiency and nature of the photochemical reaction are oxygen-independent.

Photouncaging mechanism

To elucidate the photouncaging mechanism, we carried out time-resolved absorption measurements using nanosecond laser flash photolysis, a powerful tool to gain insights into the spectroscopic and kinetic properties of transient intermediates produced by light excitation. However, before discussing these results, for the sake of clarity, we consider it helpful to briefly recall the critical aspects of the photodegradation mechanism of **NF** that was previously reported.[63–65] This FQ undergoes photodefluorination mediated by the lowest excited triplet. In the presence of a phosphate buffer, the loss of

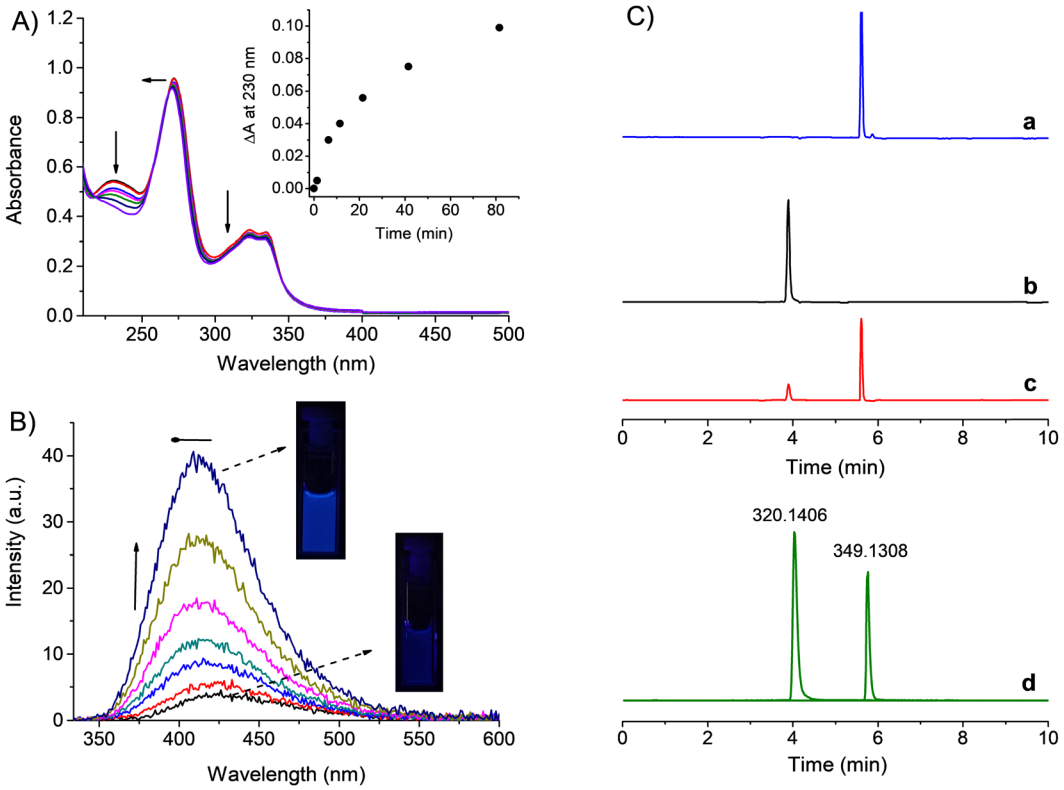

Fig. 2 (A) Absorption spectral changes observed upon exposure of a PBS solution (10 mM, pH 7.4) of **NF–NO** (40 μM) at λ_{exc} = 420 nm (*ca.* 20 mW cm^{-2}) for time intervals from 0 to 81 min. The arrows indicate the course of the spectral profile with the illumination time. The inset shows the difference absorbance changes at λ = 230 nm. (B) Evolution of the fluorescence emission spectra corresponding to the sample of (A) and recorded at λ_{exc} = 324 nm. The inset shows the actual images of the solution acquired before and after the photolysis. (C) UHPLC traces related to solutions of **NF–NO** (a), **NF** (b) and **NF–NO** after 15 min irradiation at λ_{exc} = 420 nm (*ca.* 20 mW cm^{-2}) (c) recorded at λ = 278 nm; (d) shows UHPLC traces recorded at *m*/*z* values of **NF** and **NF–NO**. *T* = 25 °C.

fluoride is triggered by the formation of the **NF** radical anion generated by an unexpected photoinduced electron transfer between the **NF** triplet state and the hydrogen phosphate dianion of the buffer, which acts as a reducing agent. The **NF** radical anion is well detectable with laser flash photolysis because it is characterized by a longer lifetime and absorption maximum in a different spectral region than the triplet precursor (Scheme 2A).[63–65]

In the case of **NF–NO**, a different scenario was observed. Fig. 4 shows the transient spectra observed with elapsing time after the initial excitation laser pulse of an **NF–NO** solution in PBS. The spectrum taken at the shortest delay time shows a maximum at *ca.* 620 nm, which agrees with the features of the lowest triplet state of **NF**. The spectral evolution reveals that no new transient species are formed concurrently with the triplet decay. Therefore, there is no evidence for the radical anion with a maximum of 720 nm. The triplet state decays monoexponentially with a lifetime $\tau \sim 1$ μs (inset Fig. 4) in reasonably good agreement with triplet decay reported for **NF**. Analogously to **NF**, this decay was dependent on the PBS with bimolecular rate constants $k_{q(PBS)} \sim 8 \times 10^7$ M^{-1} s^{-1}. This value is similar to that reported for **NF**[63] and confirms the occurrence of the bimolecular photoinduced electron transfer between the **NF–NO** triplet and the phosphate ions.

Note that, the photogeneration of NO cannot be the result of a direct excitation of the nitrosated piperazinyl moiety since it does not absorb the blue excitation light. Therefore the photouncaging mechanism illustrated in Scheme 2B and discussed in the following is proposed.

Nitrosation of the piperazinyl ring is reasonably expected not significantly to change neither the oxidation potential nor the energy of the triplet state with respect to the values reported for **NF**. Therefore, also in this case, the triplet quenching by PBS must necessarily involve the formation of **NF–NO** radical anion. We believe that the lack of observation of this species might be attributable to a second, intramolecular electron transfer between this radical anion and the nitroso group leading to a radical anion centred on the nitroso group and occurring on a time scale faster than the triplet decay. This process is expected to be exergonic or almost thermoneutral (the reduction potentials of aliphatic nitrosamine are in the range −0.5 V to −1.5 V *vs* Ag/AgCl, depending on the conditions[66,67] whereas that of the aromatic core of **NF** is reported to be *ca.* −1.4 V *vs.* Ag/AgCl[63]) and can be also favoured by the close spatial proximity between the FQ core and the nitroso-piperazinyl moiety. The formation of NO-centred radical anion can be reasonably responsible for the release of NO and, after protonation, the restoring of **NF**. This hypothesis is supported by the fact that

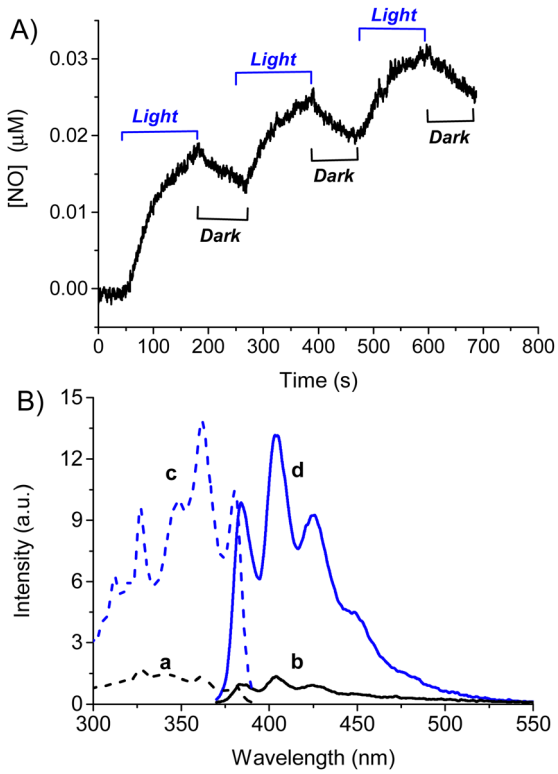

Fig. 3 (A) NO release profile observed for an air-equilibrated PBS solution (10 mM, pH 7.4) of **NF–NO** (40 μM) upon alternate cycles of light irradiation at λ_{exc} = 405 nm. T = 25 °C. (B) Fluorescence emission (solid lines) and excitation (dotted lines) spectra obtained after fluorimetric assay of PBS solutions (10 mM, pH 7.4) of **NF–NO** (40 μM) before (a) and (b) and after (c) and (d) 30 min irradiation with blue light at 420 nm. The emission wavelength for the excitation spectra was 410 nm whereas the excitation wavelength for the emission spectra was 360 nm. T = 25 °C.

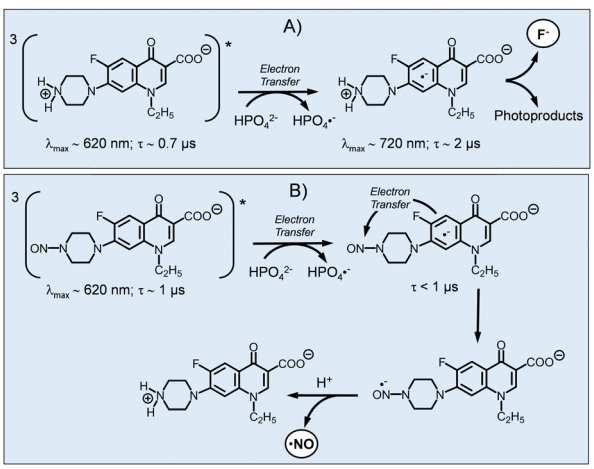

Scheme 2 (A) Photodefluorination mechanism of **NF** in PBS solution at pH 7.4. (B) Proposed mechamism for **NF** and NO photouncaging from **NF–NO** in PBS solution at pH 7.4.

radical anions of nitroso-derivatives possess a lower dissociation energy of the N–NO bond than their neutral form, encouraging fast NO detachment.[68] This proposal accords well with the

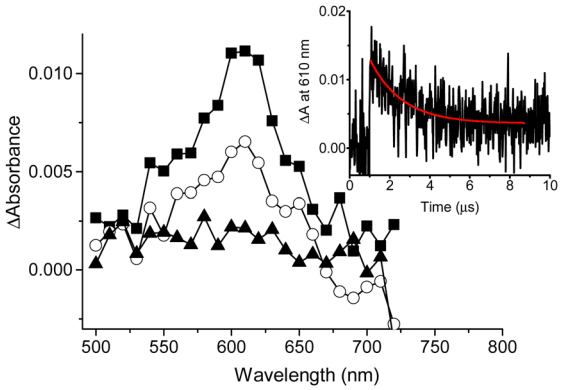

Fig. 4 Transient absorption spectra observed 0.1 μs (■), 0.5 μs (○) and 8 μs (▲) after 355 nm laser excitation (E_{355} ~ 10 mJ pulse^{-1}) of N_2-saturated PBS solution (10 mM, pH 7.4) of **NF–NO** (40 μM). The inset shows the decay trace monitored at 610 nm and the related first-order fitting.

negligible photogeneration of NO observed when photolysis was carried out in neat water in the absence of PBS. This finding confirms the key role of the buffer as external reducing agent in the photouncaging process and rules out a photouncaging mechanism involving the formation of a NO-centered radical anion by an intramolecular electron transfer between the photoexcited FQ core and the nitroso-piperazinyl moiety.

The mechanism of Scheme 2B implies a photodecaging strictly dependent on the presence of phosphate buffer as reducing agent as initiator of the stepwise process. This condition may, in principle, represent a not negligible limitation. Therefore, we wondered if the photouncaging process can be triggered by biological reducing agents analogously to what observed for phosphate ions. To this end, we devised laser flash photolysis experiments with **NF–NO** in neat water in the absence of PBS but in the presence of a tyrosine (TyrOH), used as representative example of an amino acid commonly present in biological samples. The rationale behind this experiment is that TyrOH not only is a better reducing agent than phosphate ion but, if an electron transfer with the **NF–NO** triplet occurs, it is expected to generate a tyrosyl radical (TyrO$^{\bullet}$). Analogously to others phenoxyl radicals, this species is well detectable by transient spectroscopy due to its absorption around 400 nm (where the triplet absorption of **NF–NO** is negligible) and the decay in the tens of microseconds time regime,[69] and would elegantly confirm the proposed mechanism.

Fig. 5A shows the transient spectra taken at 2 different delay time with respect to the initial laser pulse. They clearly show that the decay of the **NF–NO** triplet at 620 nm is accompanied by a build-up of a new absorption showing the characteristic features of the TyrO$^{\bullet}$ radical[70] which decays *via* second-order kinetic on longer temporal scale. As shown in the Fig. 5B, although affected by the fluorescence emission on this short time scale, the decay of the triplet monitored at 620 nm matches very well the build-up of the tyrosyl radical at 390 nm with an observed rate constant k_{obs} ~ 1.6 × 10^6 s^{-1}. This confirms that TyrO$^{\bullet}$ radical is generated by intermolecular electron transfer between **NF–NO** triplet and TyrOH and,

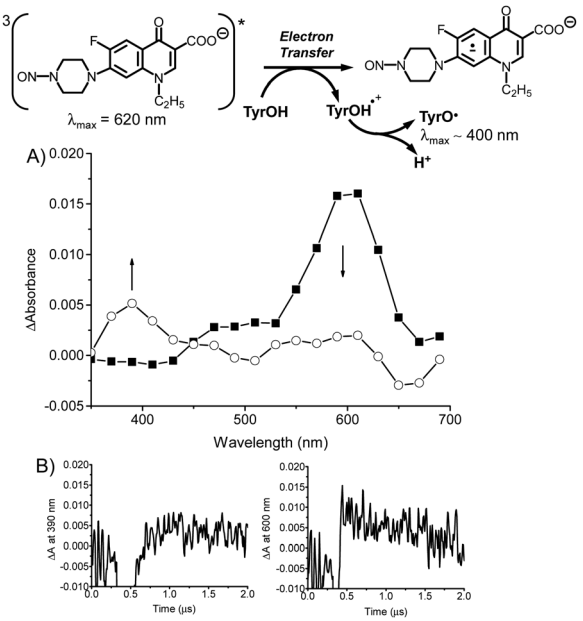

Fig. 5 (A) Transient absorption spectra observed 0.2 μs (■) and 1.5 μs (○) after 355 nm laser excitation (E_{355} ~ 10 mJ pulse^{-1}) of N_2-saturated aqueous solution of **NF–NO** (40 μM) in the presence of TyrOH (800 μM). T = 25 °C. The inset illustrates the bimolecular electron transfer involved. (B) Build-up (left) and decay (right) traces monitored at 390 and 600 nm, respectively.

according with literature, after the concomitant fast deprotonation of the very acid TyrOH$^{\bullet+}$ radical cation (pK$_a$ = −2) (see inset Fig. 5A).[71]

Based on this value and the concentration of the TyrOH used in the experiments, a bimolecular quenching constant for this electron transfer process of $k_{q(TyrOH)} \sim 1.9 \times 10^9$ M^{-1} s^{-1} can be estimated. Note that, this value is more than one order of magnitude higher than that observed for the phosphate buffer ($k_{q(PBS)} \sim 8 \times 10^7$ M^{-1} s^{-1}) and it is in excellent agreement with the highly favoured thermodynamic associated to this process if compared with the almost thermoneutral quenching by phosphate (the potential of the couple TyrOH$^{\bullet+}$/TyrOH[70,71] is at least 0.5 V lower than that of the couple $HPO_4^{\bullet-}/HPO_4^{2-}$).

After this initial electron transfer involving TyrOH, the uncaging process is expected to proceed in the same way as reported in Scheme 2. This was confirmed by the steady-state photolysis experiments carried out in the presence of TyrOH. The intense absorption of TyrOH below 270 nm did not allow to follow the bleaching of the 230 nm band typical of **NF–NO** (see Fig. 2A). However, Fig. S7 (ESI†) shows the fluorescence intensity increase accompanied by the shift of the emission maximum upon photolysis with blue light. This photolysis profile is the same as observed in the presence of PBS (see Fig. 2B), and it provided unambiguous evidence for the uncaging of **NF** under these conditions. In parallel, the trapping experiment performed with the DAN confirmed the simultaneous generation of NO (Fig. S8, ESI†).

The last quantitative aspect that deserves to be highlighted is the reliability of the value of *ca.* 0.1 estimated for Φ_u (*vide supra*) for a triplet-mediated reaction. If this is the case, the quantum yield for the triplet formation, Φ_T, should be $> \Phi_u$. To this end, we determined the Φ_T value by performing a laser power effect on the top ΔA of the **NF–NO** triplet and, for comparison, of **NF**, for which a value of $\Phi_T > 0.5$ has been reported. The slopes of the data set reported in Fig. S9 (ESI†) are proportional to the product $\Phi_T \times \varepsilon_{T-T}$, where ε_{T-T} is the triplet molar absorption coefficient. By taking into account that the solutions are iso-absorbing at the excitation wavelength and that large changes in the ε_{T-T} are reasonably unlikely, being substantially unchanged the band profiles, a $\Phi_T > 0.17$ for **NF–NO** can be directly estimated by the different slopes of the straight lines obtained from the linear portion of the plots.

Biological studies

Previous studies have reported that the MIC of **NF–NO** is 2 to 38-fold higher than that of **NF** for several different bacteria.[63] This was also confirmed by preliminary biological studies performed in this work in which **NF–NO** and, for comparison, **NF** were tested against ATCC *S. aureus* in the dark and under blue light irradiation. As shown in Table 1, the MIC value of **NF–NO** is *ca.* 4-fold higher than that found for **NF**. Interestingly, while the MIC value of NF did not change upon irradiation, that of **NF–NO** reduced by about 50% after only 10 min irradiation, according to the release of the more active **NF** and NO.

As emphasized above, another remarkable point of this work is the possibility of real-time monitoring of the release process thanks to the highly fluorescent **NF**, photoliberated by the low fluorescent **NF–NO**, which acts as self-reporting. To demonstrate that the reduction of the MIC of **NF–NO** is due to the photouncaging of **NF**, we carried out fluorescence microscopy imaging experiments with a 24-hour biofilm of ATCC strain of *S. aureus* assembled on a glass coverslip and incubated with **NF–NO**. Fig. 6 shows no detectable fluorescence in the non-irradiated sample (panel a). In contrast, a significant blue emission, typical for **NF**, appears after irradiation of the sample (panel b), analogously to what was observed for the PBS solution in the absence of bacteria (see Fig. 2B and related pictures). Moreover, since the emission of **NF** presents a tail that extends up to the green region (see Fig. 2B), the fluorescence in bacteria can also be monitored in the green channel (panel c).

These findings unequivocally demonstrate the formation of the active **NF** and, consequently, the release of NO under these experimental conditions, suggesting an excellent preservation of the photobehaviour of **NF–NO** even in the presence of bacterial cells. It should be stressed that the retention of the photochemical properties after incubation of photoactivatable components with biological systems is not trivial. Several factors,

Table 1 MIC of **NF** and **NF–NO** against ATCC *S. aureus* in the dark and after 10 min irradiation with blue light at 420 nm

Sample	MIC (μg mL^{-1}) dark	MIC (μg mL^{-1}) light
NF	0.39	0.39
NF–NO	1.56	0.78

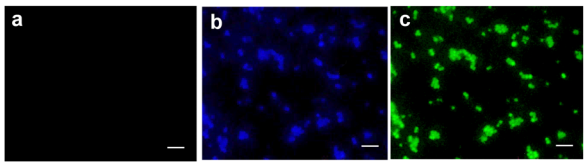

Fig. 6 Confocal fluorescence microscopy images of ATCC strain of *S. aureus* biofilm incubated with **NF–NO** in the dark (a) and after 15 min irradiation with blue light (b) and (c), and monitored in the blue (a) and (b) and the green channel (c). λ_{exc} = 405 nm. Scale bar: 5 μm.

such as the micropolarity of the medium, steric constraints, and specific interactions, may often lead the specific photoresponsive compound forming supramolecular assemblies exhibiting significant changes in the primary photochemical process.

Conclusions

We successfully demonstrated that the temporary inactivation of the FQ antibacterial **NF** through its conversion into the nitrosated derivative **NF–NO** might represent an intriguing photopharmacological approach to simultaneously liberate the active **NF** and the unconventional antibacterial NO with high spatiotemporal precision under the exclusive control of visible blue light. The mechanism of photorelease probably occurs through a two-step inter-and intramolecular electron transfer initiated by the lowest triplet state of **NF–NO** and the phosphate buffer ions as reducing agents. This mechanism not only permits the simultaneous generation of a conventional and an ''unconventional'' antibacterial species under light control but significantly suppresses the photodefluorination process typical for **NF** and other FQs, which is the primary process responsible for the phototoxic and photocarcinogenic side effects. Another remarkable value of this approach is that the typical fluorescence emission of **NF** is quenched in **NF–NO**, and it is wholly restored upon **NF** photouncaging, making **NF** an effective optical self-reporter to monitor the photorelease in real-time with the aid of fluorescence techniques. Notably, the photouncage mechanism also operates without phosphate buffer but in the presence of biologically relevant reducing components such tyrosine, and is well preserved in bacteria cells where a significant reduction of the MIC of **NF–NO** is observed upon irradiation due to the release of **NF** and NO. To our knowledge, this represents the first example of FQ acting as a photocage to uncage itself and generate NO.

The presence of piperazinyl appendages possessing secondary amine is quite common in the structure of many FQs. Besides, the photochemical reactivity of this class of compounds has been, in most cases, well-elucidated. Taking this into account, the present work might, in principle, open up unexplored opportunities in antibiotic photopharmacology, exploiting the nitrosation as a facile route to cage NO, switching OFF the pharmacological action of the FQs, and using light as a remote activation mechanism to uncage the active antibiotic drug and NO with high spatiotemporal control. Studies in this direction will be the object of further investigations.

Data availability

Data for this article, including [Fig. 1–6] are available at [Zenodo at **https://Zenodo.org**].

Conflicts of interest

No conflicts to declare.

Acknowledgements

We thank HORIZON-MSCA-2021-PF-01, 101057562 – SUPREME for financial support to MC fellow T. J. M. and research funding. JGP – FAPESP – 2022/10251-0, IPRB – Coordination for the Improvement of Higher Education Personnel – Brazil (CAPES) – Finance Code 001.

Notes and references

1 World Health Organization. Antimicrobial resistance. A manual for developing national action plans. chrome-extension://efaidnbmnnnibpcajpcglclefindmkaj/https://iris.who.int/bitstream/handle/10665/204470/9789241549530_eng.pdf?sequence = 1(accessed May 17, 2024).
2 Antimicrobial Resistance: Tackling a Crisis for the Future Health and Wealth of Nations, **https://amr-review.org/** (accessed May 17, 2024).
3 World Health Organization, Antimicrobial Resistance: Global Report on Surveillance; World Health Organization, **https://www.who.int/publications/i/item/9789241564748** (accessed May 17, 2024).
4 C. J. Murray, K. S. Ikuta, F. Sharara, L. Swetschinski, G. R. Aguilar, A. Gray, C. Han, C. Bisignano, P. Rao, E. Wool and S. C. Johnson, *Lancet*, 2022, **399**, 629–655.
5 Q. A. Duong, L. F. Pittet, N. Curtis and P. Zimmermann, *J. Infect.*, 2022, **85**, 213–300.
6 G. Dubourg, J. C. Lagier, C. Robert, F. Armougom, P. Hugon, S. Metidji, N. Dione, N. P. M. Dangui, A. Pfleiderer, J. Abrahao, D. Musso, L. Papazian, P. Brouqui, F. Bibi, M. Yasir, B. Vialettes and D. Raoult, *Int. J. Antimicrob. Agents*, 2014, **44**, 117–124.
7 D. V. Patangia, C. A. Ryan, E. Dempsey, R. P. Ross and C. Stanton, *MicrobiologyOpen*, 2022, **11**, 1–23.
8 F. S. Del Fiol, V. M. Balcão, S. Barberato-Fillho, L. C. Lopes and C. C. Bergamaschi, *Front. Pharmacol.*, 2018, **9**, 1–10.
9 D. C. Nwobodo, M. C. Ugwu, C. O. Anie, M. T. S. Al-Ouqaili, J. C. Ikem, U. V. Chigozie and M. Saki, *J. Clin. Lab. Anal.*, 2022, **36**, 1–10.
10 M. M. Lerch, M. J. Hansen, G. M. van Dam, W. Szymanski and B. L. Feringa, *Angew. Chem., Int. Ed.*, 2016, **55**, 10978–10999.
11 W. A. Velema, W. Szymanski and B. L. Feringa, *J. Am. Chem. Soc.*, 2014, **136**, 2178–2191.
12 I. M. Welleman, M. W. H. Hoorens, B. L. Feringa, H. H. Boersma and W. Szymanski, *Chem. Sci.*, 2020, **11**, 11672–11691.

13 M. J. Fuchter, *J. Med. Chem.*, 2020, **63**, 11436–11447.
14 S. Sortino, *J. Mater. Chem.*, 2012, **22**, 301–318.
15 M. R. Hamblin and T. Hasan, *Photochem. Photobiol. Sci.*, 2004, **3**, 436–450.
16 P. R. Ogilby, *Chem. Soc. Rev.*, 2010, **39**, 3181–3209.
17 P. Agostinis, K. Berg, K. A. Cengel, T. H. Foster, A. W. Girotti, S. O. Gollnick, S. M. Hahn, M. R. Hamblin, A. Juzeniene, D. Kessel, M. Korbelik, J. Moan, P. Mroz, D. Nowis, J. Piette, B. C. Wilson and J. Golab, *CA - Cancer J. Clin.*, 2011, **61**, 250–281.
18 A. M. Emmerson and A. M. Jones, *J. Antimicrob. Chemother.*, 2003, **51**, 13–20.
19 P. C. Appelbaum and P. A. Hunter, *Int. J. Antimicrob. Agents*, 2000, **16**, 5–15.
20 E. R. Vlieghe, J. A. Jacobs, M. Van Esbroeck, O. Koole and A. VanGompel, *J. Travel Med.*, 2008, **15**, 419–425.
21 U.S. Food and Drug Administration, FDA updates warnings forfluoroquinolone antibiotics, **https://www.fda.gov/NewsEvents/Newsroom/PressAnnouncements/ucm513183.htm** (accessed May 17, 2024).
22 J. Ferguson, *Photochem. Photobiol.*, 1995, **62**, 954–958.
23 G. Klecak, F. Urbach and H. Urwyler, *J. Photochem. Photobiol., B*, 1997, **37**, 174–181.
24 A. A. Chatelat, S. Albertini and E. Gocke, *Mutagenesis*, 1996, **11**, 497–504.
25 M. Makinen, P. D. Forbes and F. Stenbaeck, *J. Photochem. Photobiol., B*, 1997, **37**, 182–187.
26 L. J. Martinez and C. F. Chignell, *J. Photochem. Photobiol., B*, 1998, **45**, 51–59.
27 L. J. Martinez, G. Li and C. F. Chignell, *Photochem. Photobiol.*, 1997, **65**, 599–602.
28 L. J. Martinez, R. H. Sik and C. F. Chignell, *Photochem. Photobiol.*, 1998, **67**, 399–403.
29 S. Sortino, G. De Guidi, S. Giuffrida, S. Monti and A. Velardita, *Photochem. Photobiol.*, 1998, **67**, 167–173.
30 G. Zhang and P. Wan, *J. Chem. Soc., Chem. Commun.*, 1994, **1**, 19–20.
31 W. A. Velema, J. P. van der Berg, W. Szymanski, A. J. Driessen and B. L. Feringa, *ACS Chem. Biol.*, 2014, **9**, 1969–1974.
32 W. A. Velema, J. P. van der Berg, M. J. Hansen, W. Szymanski, A. J. M. Driessen and B. L. Feringa, *Nat. Chem.*, 2013, **5**, 924–928.
33 W. A. Velema, M. J. Hansen, M. M. Lerch, A. J. M. Driessen, W. Szymanski and B. L. Feringa, *Bioconjugate Chem.*, 2015, **26**, 2592–2597.
34 M. Wegener, M. J. Hansen, A. J. Driessen, W. Szymanski and B. L. Feringa, *J. Am. Chem. Soc.*, 2017, **139**, 17979–17986.
35 S. Bhunia, A. Das, S. K. Jana, S. Mandal and S. Samanta, *Bioconjugate Chem.*, 2024, **35**, 92–98.
36 S. Bhunia, S. K. Jana, S. Sarkar, A. Das, S. Mandal and S. Samanta, *Chem. Eur. J*, 2024, **30**, e2023036.
37 G. Du, J. Fu, Y. Zheng, F. Hu, X. Shen, B. Li, X. Zhao and Z. Yu, *Org. Biomol. Chem.*, 2023, **21**, 1021–1026.
38 P. Kumari, A. Kulkarni, A. K. Sharma and H. Chakrapani, *ACS Omega*, 2018, **3**, 2155–2160.
39 Y. Shi, V. X. Truong, K. Kulkarni, Y. Qu, G. P. Simon, R. L. Boyd, P. Perlmutter, T. Lithgow and L. S. Forsythe, *J. Mater. Chem. B*, 2015, **3**, 8771–8774.
40 E. Contreras-García, C. Lozano, C. García-Iriepa, M. Marazzi, A. H. Winter, C. Torres and D. Sampedro, *Pharmaceutics*, 2022, **14**, 2–13.
41 L. J. Ignarro, *Nitric Oxide: Biology and Pathobiology*, Academic Press, 2010.
42 L. J. Ignarro, *Arch Pharm Res.*, 2009, **32**, 1099–10100.
43 G. G. Fang, *Nitric Oxide and Infections*, Kluwer Academic/Plenum Publishers, 1999.
44 F. C. Fang, *J. Clin. Invest.*, 1997, **99**, 2818–2825.
45 D. O. Schairer, J. S. Chouake, J. D. Nosanchuk and A. J. Friedman, *Virulence*, 2012, **3**, 271–279.
46 P. R. Gardner, A. M. Gardner, L. A. Martin and A. L. Salzman, *Proc. Natl. Acad. Sci. U. S. A.*, 1998, **95**, 10378–10383.
47 F. C. Fang, *Nat. Rev. Microbiol.*, 2004, **2**, 820–832.
48 Q. Jia, A. J. Janczuk, T. Cai, M. Xian, Z. Wen and P. G. Wang, *Expert Opin. Ther. Patents.*, 2002, **12**, 819–826.
49 S. Sortino, *Chem. Soc. Rev.*, 2010, **39**, 2903–2913.
50 P. C. Ford, *Coord. Chem. Rev.*, 2018, **376**, 548–564.
51 N. L. Fry and P. K. Mascharak, *Acc. Chem. Res.*, 2011, **44**, 289–298.
52 N. Ieda, Y. Oka, T. Yoshihara, S. Tobita, T. Sasamori, M. Kawiguchiand and H. Nakagawa, *Sci. Rep.*, 2019, **9**, 1–8.
53 A. Fraix, C. Parisi, M. Seggio and S. Sortino, *Chem. – Eur. J.*, 2021, **27**, 12714–12725.
54 A. Fraix, N. Marino and S. Sortino, *Topics in Curr. Chem.*, 2016, **370**, 225–257.
55 S. Sortino and G. Condorelli, *New J. Chem.*, 2002, **26**, 250–258.
56 S. Sortino, G. De Guidi and S. Giuffrida, *New J. Chem.*, 2001, **25**, 197–199.
57 S. Sortino, *Photochem. Photobiol.*, 2006, **82**, 64–70.
58 S. Monti, S. Sortino, E. Fasani and A. Albini, *Chem. – Eur. J.*, 2001, **7**, 2185–2196.
59 G. Condorelli, G. De Guidi, S. Giuffrida, S. Sortino, R. Chillemi and S. Sciuto, *Photochem. Photobiol.*, 1999, **70**, 280–286.
60 R. A. Lawrenson and J. W. Logie, *J. Antimicrob. Chemother.*, 2001, **48**, 895–901.
61 A. Bhaumik, *Ind. Vet. J.*, 1997, **74**, 246–247.
62 L. H. Sumano, C. L. Ocampo, G. W. Brumbaugh and R. E. Lizarraga, *Br. Poult. Sci.*, 1998, **39**, 42–46.
63 M. D. Adjei, T. M. Heinze, J. Deck, J. P. Freeman, A. J. Williams and J. B. Sutherland, *Appl. Environ. Microbiol.*, 2006, **72**, 5790–5793.
64 E. Fasani, M. Mella, S. Monti and A. Albini, *Eur. J. Org. Chem.*, 2001, 391–397.
65 A. Albini and S. Monti, *Chem. Soc. Rev.*, 2003, **32**, 238–250.
66 X. Su, L. Bromberg, K.-J. Tan, T. F. Jamison, L. P. Padhye and T. A. Hatton, *Environ. Sci. Technol. Lett.*, 2017, **4**, 161–167.
67 S. Toma, A. Omosebi, X. Gao, K. Abad, S. Bhatnagar, D. Qian, K. Liu and J. G. Thompson, *Chemosphere*, 2023, **333**, 1–11.

68 X. Q. Zhu, J.-Q. He, Q. Li, M. Xian, J. Lu and J.-P. Cheng, *J. Org. Chem.*, 2000, **65**, 6729–6735.
69 P. K. Das, M. V. Encinas, S. Steenken and J. C. Scaiano, *J. Am. Chem. Soc.*, 1981, **103**, 4162–4166.
70 C.-Y. Lu and Y.-Y. Liu, *Biochem. Biophys. Acta*, 2002, **1571**, 71–76.
71 J. J. Warren, J. R. Winkler and H. B. Gray, *FEBS Lett.*, 2012, **586**, 596–602.